Resistance Spot Welding of Galvanized Steel: Part II. Mechanisms of Spot Weld Nugget Formation

S. A. GEDEON and T. W. EAGAR

Dynamic inspection monitoring of the weld current, voltage, resistance, electrode displacement, and force was performed in conjunction with a detailed study of the effects of material variations and weld process parameter modifications on resistance spot welding of coated and uncoated steels. In order to determine the mechanisms of weld nugget formation and growth, scanning electron microscopy photos were taken of the developing nugget. These physical changes were then related to the dynamic inspection curves and the welding current lobe. The effects of material variations and weld process modifications, the results of which were presented in Part I, can be explained through an understanding of these mechanisms.

I. INTRODUCTION

IN Part I of this paper, results were presented on the effect of material variations and process modifications on the resistance spot weldability of zinc-coated steel sheets. For the purposes of this paper, weldability is defined as the acceptable welding current range as determined by the welding lobe as defined in Part I. Materials examined include hot-dip galvanized material with a mostly free zinc coating, galvannealed material with a fully alloyed Fe-Zn coating, and the uncoated base metal substrates. Material variations studied include zinc coating integrity, composition, thickness, surface roughness, oil, and amount and type of Fe-Zn intermetallics. Process parameter modifications studied include upsloping and downsloping of the weld current, preheat current, postheat current, applied force, and electrode tip geometry.

Part II presents the mechanisms of spot weld nugget formation and growth which will explain some of these previous results. In-process weld monitoring experiments were performed which are presented in support of these mechanisms. These experiments include dynamic resistance and displacement traces of hot-dip galvanized, galvannealed, and uncoated material. In order to determine the role of zinc coating location on the faying or electrode interfaces, dynamic inspection and lobe width data are presented for hot-dip galvanized material where the coating was removed from either the faying surface or the electrode sheet interfaces. In order to explain the process modification results, SEM, nugget growth studies, and dynamic inspection data are also presented for welds made with upsloping or downsloping of the weld current.

II. EXPERIMENTAL PROCEDURE

Scanning electron microscopy (SEM) photos were taken of a developing weld nugget so that the physical phenomena occurring at various stages of formation and growth could be monitored. The developing nuggets were examined by stopping the weld sequence at various times during a weld and breaking the two sheets apart, or cross sectioning them, to view what was happening at the faying or electrode interfaces. By doing this, a stop-action sequence can be observed of the developing weld nugget.

An Energy Dispersive X-ray Analysis (EDAX) unit attached to the SEM was used to examine the movement of the zinc and Fe-Zn alloy layers away from the weld area. This was also used to determine the amount of copper alloyed with the zinc on the electrode-sheet interface.

The effect of zinc on either the faying or electrode interfaces was investigated by stripping the zinc with HCl and water from one side of each of the steel sheets being welded. Dynamic resistance curves of the faying and electrode-sheet interface contact resistances were studied by connecting the voltage leads across the interface of interest rather than from electrode to electrode.

Measurements of the rate of weld nugget growth and the movement of the zinc halo which is pushed away from the weld area were performed on welds made using upsloping and radiused tipped electrodes. This was performed after cross sectioning of the nuggets or pulling the two sheets apart, depending on the extent of nugget formation.

Dynamic resistance and displacement monitoring was performed on all welds made throughout the above studies. The methods and equipment used for these monitoring studies are being prepared for publication. The materials used in this project were described in Part I.

III. RESULTS

A. *SEM Studies*

A stop-action sequence of the formation of a 0.56 cm (0.22 inch) minimum weld nugget in 12 cycles on hot-dipped (G90) material with truncated cone electrodes is presented in Figures 1 through 8 along with several elemental X-ray maps which show the location of iron and zinc on the faying and electrode interfaces.

Figure 1 shows that after the first cycle of a 12-cycle weld, the zinc coating at the faying interface has begun to melt partially. Note that the periphery of the electrode contact area has begun to melt as well as the center, and that the entire surface is not yet molten. Figure 2 shows that after two cycles of weld time the faying interface is completely molten. During the third cycle, the molten zinc coating

S. A. GEDEON is Welding Research Scientist, United States Army Materials Technology Laboratory, Watertown, MA 02172-0001. T. W. EAGAR is Associate Professor, Massachusetts Institute of Technology, Cambridge, MA 02139.

Manuscript submitted August 15, 1985.

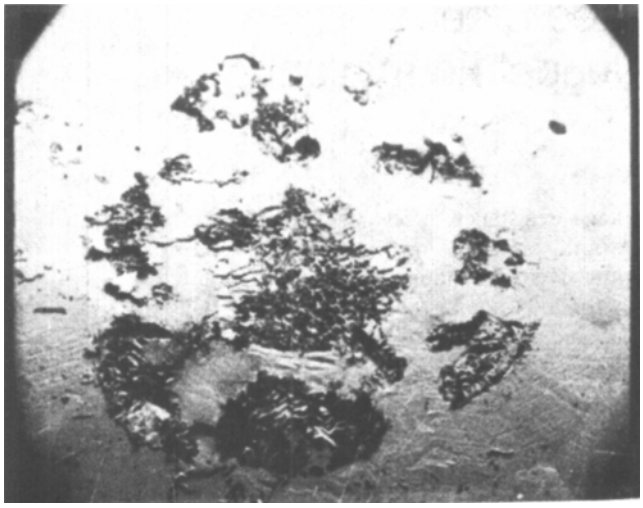

Fig. 1—Faying interface after 1 cycle of a weld which forms the minimum acceptable nugget in 12 cycles (G90, t. cone 1500 amps) showing that the zinc coating is only partially melted.

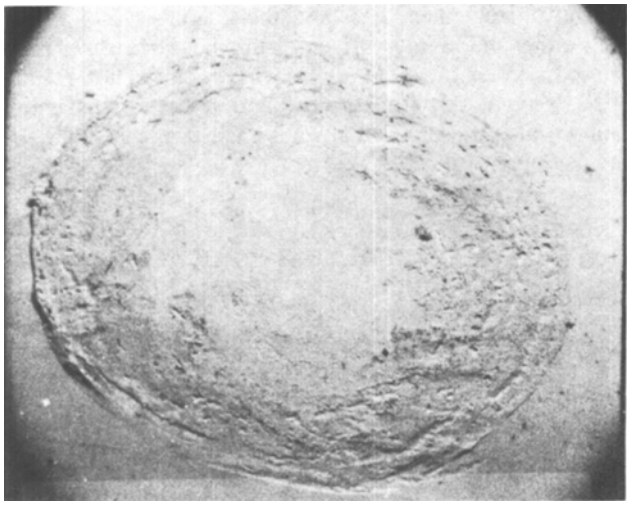

Fig. 3—Faying interface after 3 cycles of a weld which forms the minimum acceptable nugget in 12 cycles showing that the zinc coating is just starting to extrude from the center.

starts to extrude away from the electrodes and some iron-to-iron contact is seen.

The zinc coating at the electrode-sheet interface becomes molten much later than the zinc at the faying interface. Figure 4 shows that after three cycles of weld time this interface has not yet melted.

By the fifth cycle of a 12-cycle weld, the molten zinc coating at the faying interface has not been fully extruded from between the electrode tips. Figure 5 shows that a halo has not completely formed and that the molten contact area of the faying interface is larger than in the previous photos. Figure 6(a) shows that in addition to there being zinc remaining near the outer edge of the electrode periphery, there is also zinc remaining near the center of the faying interface. Figure 6(b) is an iron elemental X-ray map which shows that iron-to-iron contact is not occurring over the entire faying interface. A white dot in Figure 6(b) corresponds to the location of iron in Figure 6(a).

Figure 7(a) shows that by the seventh cycle the molten zinc halo has completely formed. Figure 7(b), a zinc elemental X-ray map, shows that some zinc has become trapped within the electrode contact area. As shown later, the molten zinc halo will continue to grow radially outward with increased time, but the trapped zinc will remain constrained in the central region unless expulsion occurs.

Figure 8 is an iron elemental X-ray map of the electrode-sheet contact area which shows that the copper electrodes can push through the zinc coating and contact the iron at the outer periphery of the electrode. The traces of the machined grooves on this relatively new electrode are easily seen. By examining the electrode-sheet interface, the amount of copper on the zinc-coated sheet was found to depend strongly on the welding schedule. Figures 9(a) and 9(b) show that very little copper is located at the sheet surface after a 12-cycle weld nugget of minimum size has formed. After 4 additional cycles of weld current, much more copper is

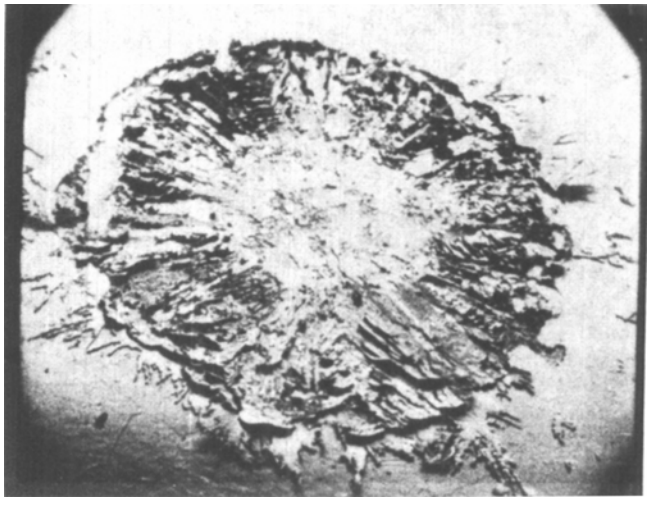

Fig. 2—Faying interface after 2 cycles of a weld which forms the minimum acceptable nugget in 12 cycles showing that the zinc coating has completely melted.

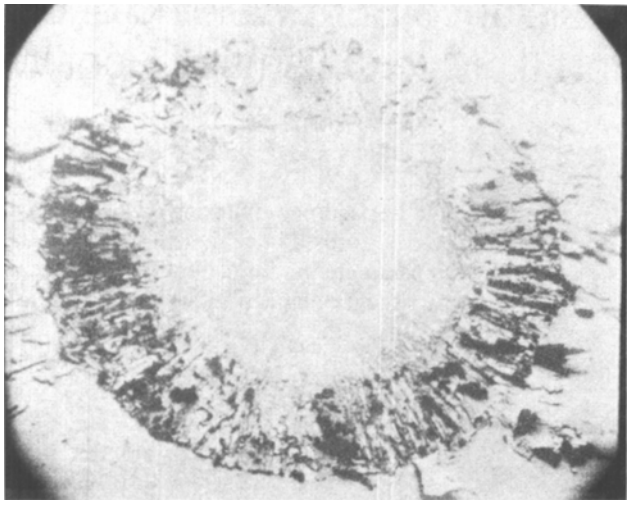

Fig. 4—Electrode interface after 3 cycles of a weld which forms the minimum acceptable nugget in 12 cycles showing that the zinc coating at this interface is not yet molten.

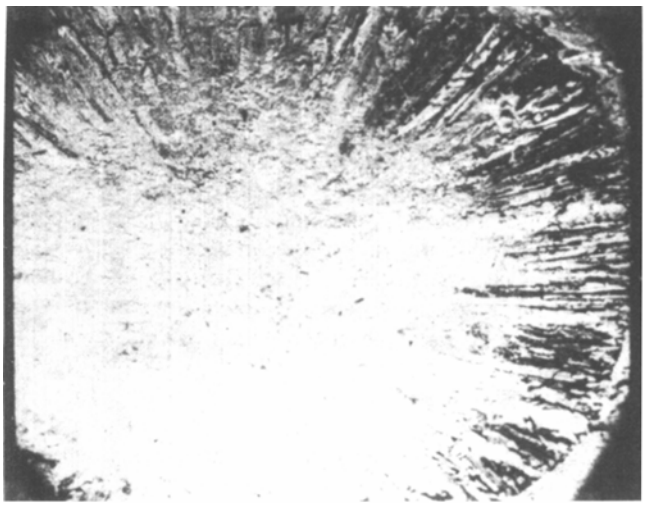

Fig. 5 — Faying interface after 5 cycles of a weld which forms the minimum acceptable nugget in 12 cycles showing that the molten zinc is substantially extruding from the center.

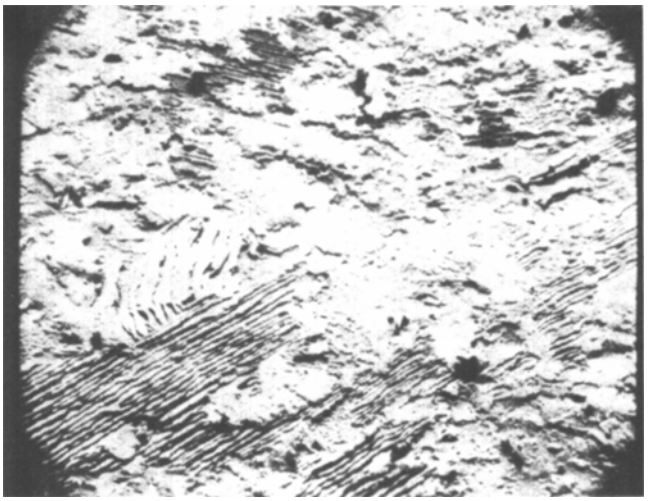

(*a*)

(*b*)

Fig. 6 — (*a*) Closeup of the center of Fig. 5 showing the presence of free zinc. (*b*) Iron elemental X-ray map corresponding to (a).

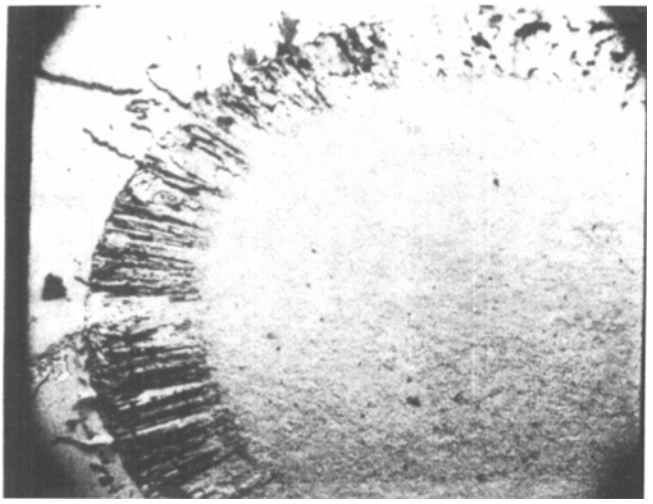

(*a*)

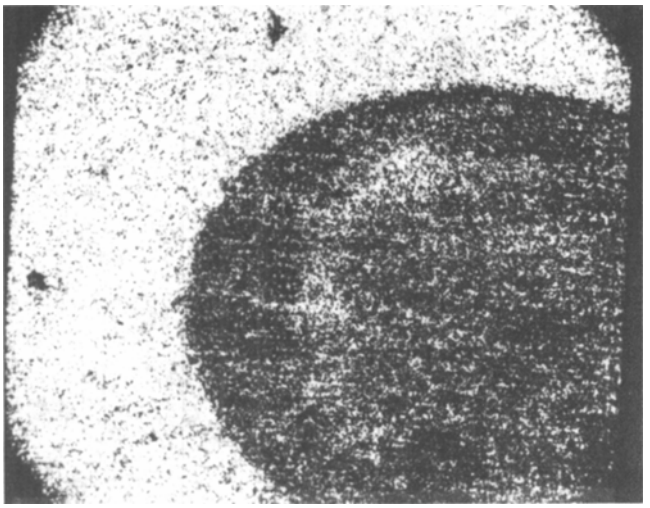

(*b*)

Fig. 7 — (*a*) Faying interface after 7 cycles of a weld which forms the minimum acceptable nugget in 12 cycles showing that a halo has now formed around the outer periphery of the weld area. (*b*) Zinc elemental X-ray map corresponding to (a) showing the presence of trapped zinc in the weld area.

found (Figure 10). If expulsion occurs, even more copper is found on the sheet surface (Figure 11).

Figure 12 shows the amount of copper on the electrode-sheet interface after 10 cycles of a weld which forms a minimum nugget at 8 cycles. The additional two cycles makes the copper pickup much worse for this short time weld than two additional cycles on a weld which forms the minimum nugget after 12 cycles. Figures 13 and 14 show that a 24-cycle weld leaves less copper even if overwelded by as much as 10 additional cycles.

Figures 15 and 16 show that by adding a few unsloped cycles, the amount of copper found on the sheet is considerably less than if no upslope were added, even if a 12-cycle weld (with 4 cycles of upslope) is overwelded by an added 12 cycles.

The above studies were also performed on heavily used electrode tips. The same trends apply, but the amount of overall alloying per weld is slightly less with the more heavily used tips.

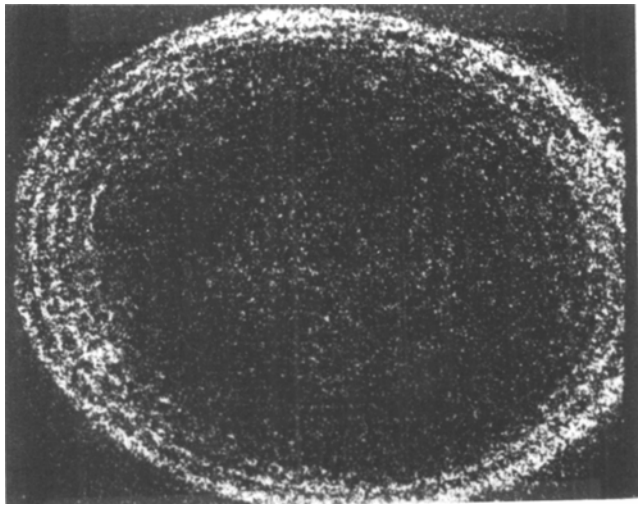

Fig. 8 — Iron elemental X-ray map of the electrode interface after 8 cycles of a weld which forms the minimum acceptable nugget in 12 cycles showing increased indentation at the periphery.

B. *Dynamic Resistance and Displacement Monitoring*

Dynamic resistance and displacement curves are presented in Figures 17 and 18 for an acceptable weld made with truncated cone electrodes on uncoated, galvannealed, and hot-dip galvanized material.

It can be seen in Figure 17(a) that the dynamic resistance of the uncoated material rises smoothly and quickly reaches a maximum before gradually decreasing. The resistance of the galvannealed material in Figure 17(b) exhibits a slight hump before it gradually increases to the maximum. The resistance decrease after the maximum was very slight for the galvannealed material. The resistance of the hot-dipped material, shown in Figure 17(c), has two humps before the final maximum. There is virtually no drop in the dynamic resistance of the hot-dipped material after the maximum is reached. Note that the value of the maximum resistance of the uncoated material is larger than the galvannealed which is larger than the hot-dipped. Also, the maximum occurs earliest for the uncoated and last for the hot-dipped material.

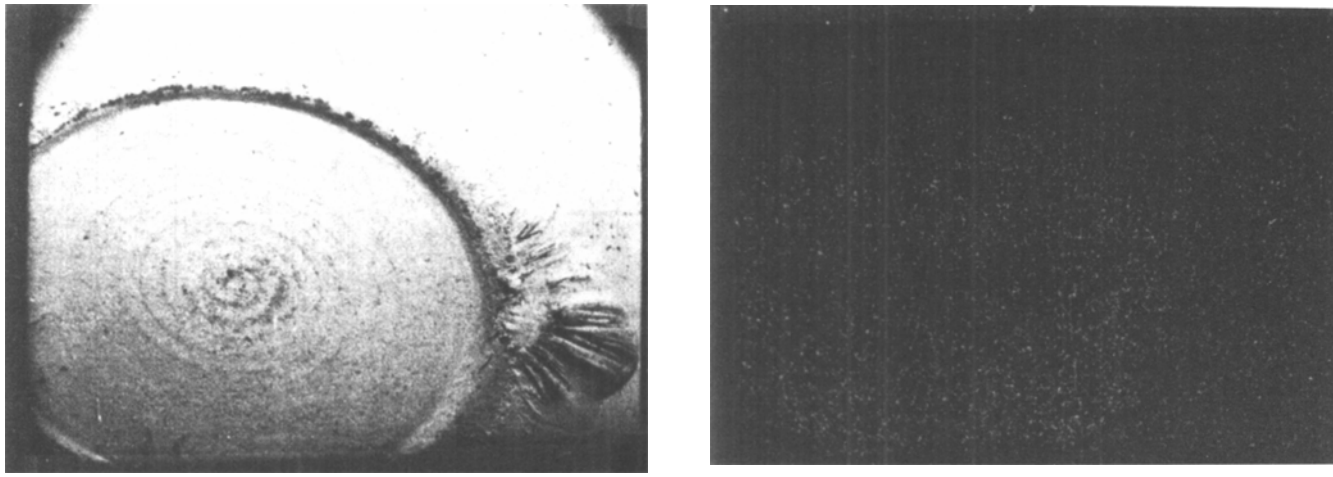

(*a*) (*b*)

Fig. 9 — (*a*) Electrode interface at completion of a 12-cycle weld. (*b*) Copper elemental X-ray map corresponding to (a).

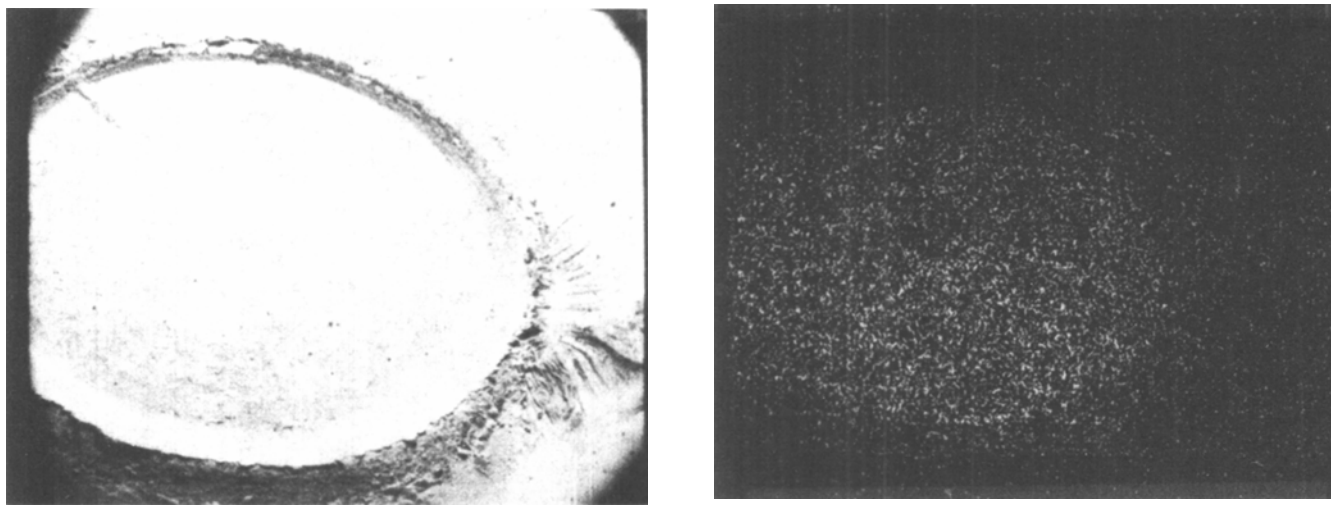

(*a*) (*b*)

Fig. 10 — (*a*) Electrode interface after 16 cycles of a weld which forms the minimum acceptable nugget in 12 cycles. (*b*) Copper elemental X-ray map corresponding to (a) showing increased amounts of copper pickup when overwelding.

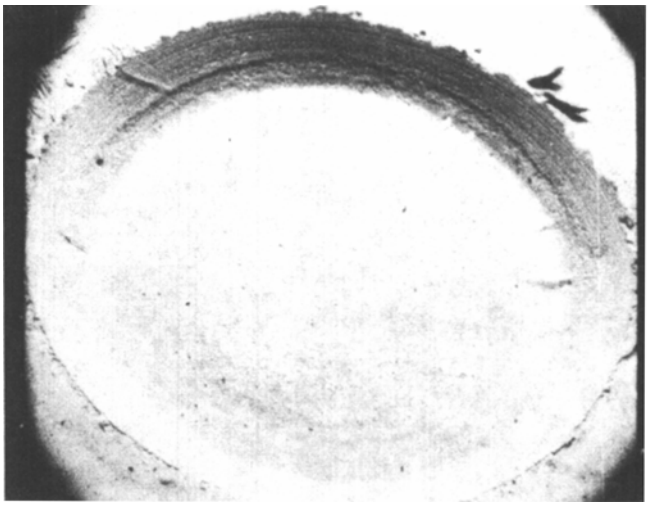

(*a*)

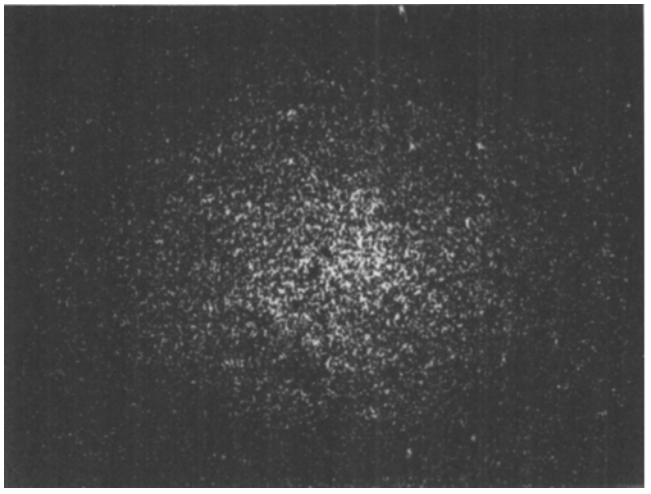

(*b*)

Fig. 11 — (*a*) Electrode interface after 16 cycles of a weld which forms the minimum acceptable nugget in 12 cycles showing increased indentation when expulsion occurs. (*b*) Copper elemental X-ray map corresponding to (a) showing increased amounts of copper pickup when expulsion occurs.

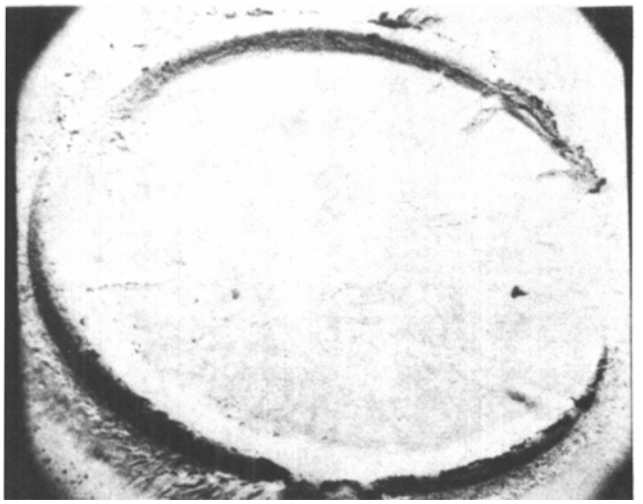

(*a*)

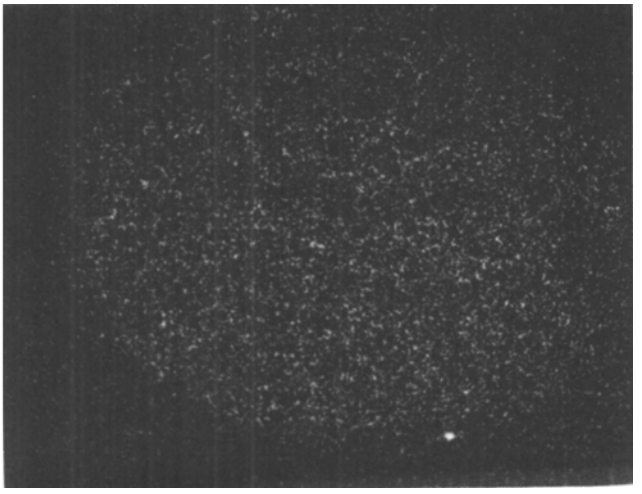

(*b*)

Fig. 12 — (*a*) Electrode interface after 10 cycles of a weld which forms the minimum acceptable nugget in 8 cycles. (*b*) Copper elemental X-ray map corresponding to (a).

The dynamic displacement of the uncoated material, shown in Figure 18(a), quickly increases to a maximum before decreasing. The displacement trace for the galvannealed material in Figure 18(b) gradually increases and sometimes exhibits a flat region before finally reaching a maximum shortly before the weld current is shut off. The hot-dipped material exhibits a hump in the displacement trace before reaching its maximum. Once again, the value of the maximum displacement is largest for the uncoated material, and smallest for the hot-dipped material.

The effects of 4 cycles of upsloped current on the resistance and displacement curves are shown in Figures 19 and 20 for G90 material with truncated cone electrodes. As can be seen, upsloping makes the resistance curve decrease for some time before sharply reaching a maximum. The use of upsloping eliminated the second hump in the dynamic resistance. The first hump in the dynamic displacement curve is reduced when upsloping is used. Upsloping had little effect on the dynamic resistance and displacement traces when welding either the galvannealed or uncoated material with truncated cone electrodes.

Dynamic resistance and displacement curves when welding with radiused tip electrodes are presented in Figures 21(a) and 22(a) for hot-dipped material, and Figures 21(b) and 22(b) for galvannealed material. The effect of upsloping on hot-dipped material with radiused tips is shown in Figures 21(c) and 22(c). All of the humps are more pronounced than when welding with truncated cone electrodes. Also, the second hump comes earlier for the resistance traces of radiused tip electrodes. Once again, upsloping reduces the size of the humps.

C. *Effect of Zinc Coating on the Faying and Electrode Interfaces*

In order to quantify the effect of zinc coating location, welds were made with zinc present at only the faying interface, only the electrode-sheet interfaces, all of the interfaces, or at none of the interfaces. A tabulation of the lobe widths measured at 12 cycles and the effect of up- and downsloping are presented in Table I.

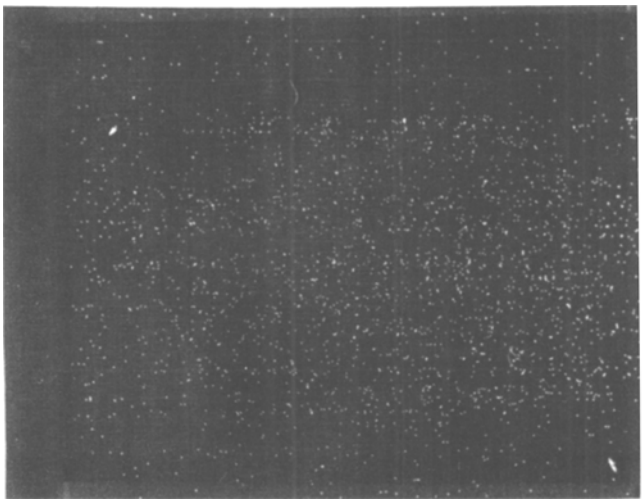

Fig. 13—Copper elemental X-ray map of the electrode interface after 28 cycles of a weld which forms the minimum acceptable nugget in 24 cycles.

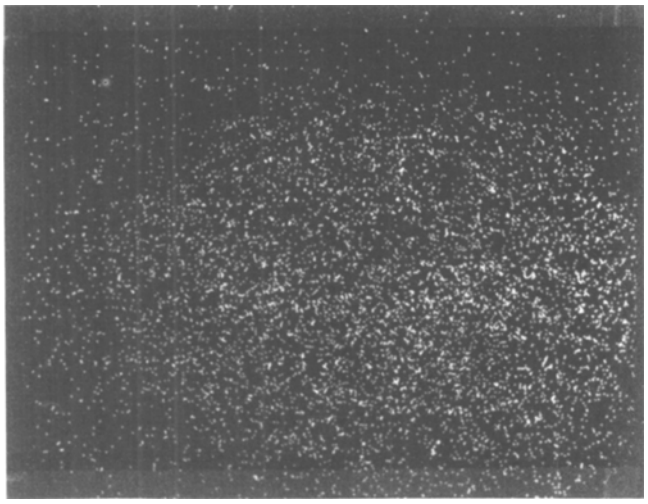

Fig. 14—Copper elemental X-ray map of the electrode interface after 34 cycles of a weld which forms the minimum acceptable nugget in 24 cycles. Note the slight copper pickup after 10 cycles of overwelding.

It was found that hot-dipped material with zinc on only the electrode interfaces had a greater lobe width than regularly coated material. Upsloping did not increase this width very much, but downsloping did by about 1000 amps. G90 with zinc on only the faying interface had a smaller lobe width than regular G90. Upsloping increased this width by about 1000 amps, and downsloping increased the width by about 1500 amps.

The uncoated material normally (without slope control) had a wider lobe width than the coated products; thus, it was quite unexpected that by stripping away zinc from the electrode interfaces the lobe width would be decreased. The currents needed for a minimum-sized nugget are about equivalent, but the expulsion current is much lower for the G90 with zinc only at the faying interface.

The dynamic resistance and displacement traces shown in Figures 23(a) and 24(a) correspond to traces of hot-dipped material with zinc on the electrode interfaces only. Figures 23(b) and 24(b) show the same material with four cycles of upsloping added. Figures 25 and 26 show similar traces with zinc present at the faying interface only. By comparing these traces with those of uncoated and regularly coated material, in Figures 17 and 18, a number of differences can be noted which depend on zinc location. The resistance increases quickly and then decreases for the material with zinc only on the electrode-sheet interfaces, whereas the resistance increases much more gradually for a material with zinc only on the faying interface. When using upslope, the material with zinc at the electrode-sheet interfaces gradually increases, whereas material with zinc only at the faying interface decreases sharply. The dynamic displacement traces of material with zinc at only the faying interface closely resembles the trace for an uncoated material. The displacement traces of material with zinc only on the electrode-sheet interfaces exhibit humps similar to those of a normally coated hot-dipped material.

The experiments performed on galvannealed material had very similar results, but not as pronounced. Also, slope

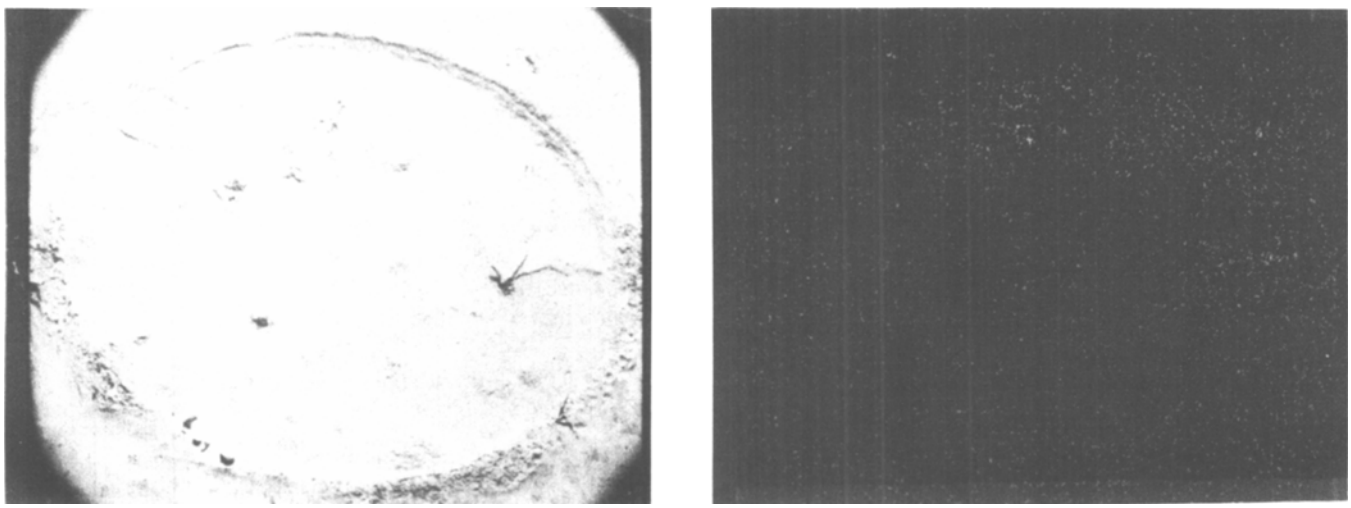

(*a*) (*b*)

Fig. 15—(*a*) Electrode interface after 16 cycles and 4 cycles upslope (acceptable weld nugget would have formed with this current after 12 cycles and no upslope). (*b*) Copper elemental X-ray map corresponding to (a).

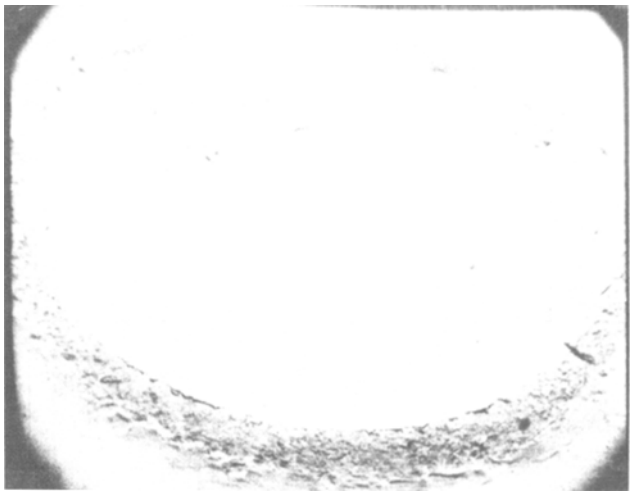

(*a*)

(*b*)

Fig. 16—(*a*) Electrode interface after 24 cycles and 4 cycles upslope (acceptable weld nugget would have formed with this current after 12 cycles and no upslope). (*b*) Copper elemental X-ray map corresponding to (a). Note the slight copper pickup after overwelding by 12 cycles and having 4 cycles of upslope in addition. Compare with Figs. 10(b) and 11(b).

control showed no effect, as was expected for either a galvannealed or uncoated material.

Figure 27 shows an example of the dynamic resistance obtained for each of the interfaces when using regularly coated G90 welded with truncated cone electrodes. As can be seen, all of the features which make up the total dynamic resistance seem to be associated with the electrode-sheet interfaces and not with the faying interface.

D. *Weld Nugget and Halo Growth Studies*

The rate of movement of the ring of melted zinc which is pushed away from the weld area between the electrode tips during welding (the halo) was measured as well as the rate of weld nugget growth. The regions measured are shown in Figure 28.

Figure 29 shows how the rates of halo and nugget growth are affected by upsloping and weld time. It can be seen that the distance between the molten iron (Dn) and molten zinc (Di) is increased due to upsloping and that the rate of nugget growth is made more even and consistent.

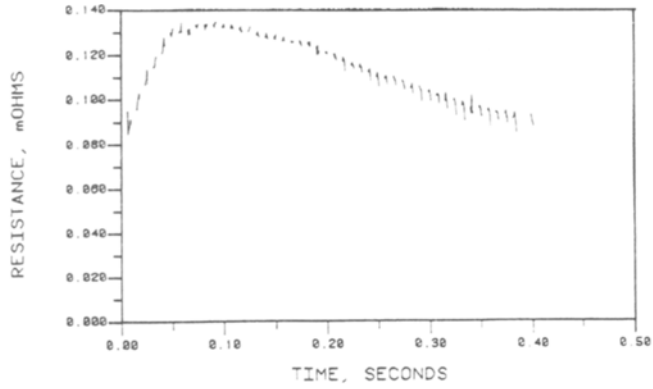

(*a*)

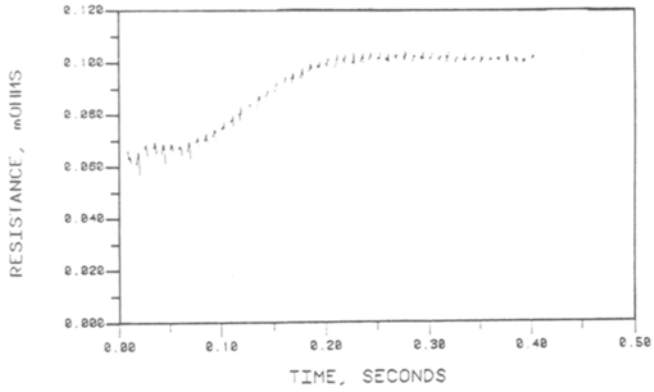

(*b*)

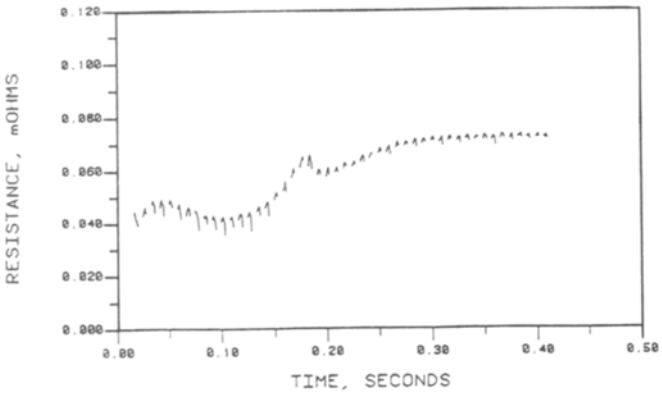

(*c*)

Fig. 17—(*a*) Dynamic resistance curve for uncoated steel (t. cone, 24 cycles, 9000 amps). (*b*) Dynamic resistance curve for galvannealed steel (t. cone, 24 cycles, 12,000 amps). (*c*) Dynamic resistance curve for hot-dipped galvanized (t. cone, 24 cycles, 12,000 amps).

IV. DISCUSSION

A. *Mechanisms of Weld Nugget Formation and Growth*

The mechanisms of weld nugget formation and growth seen in the SEM photographs can best be explained by describing what effect they have on observable phenomena such as dynamic resistance and displacement information. Features in the dynamic traces of all three types of material studied can be explained with the aid of the generalized resistance and displacement curves in Figures 30 and 31.

The generalized dynamic resistance curve can be separated into 8 distinct regions, and the displacement curve into 6 regions. From a comparison of Figures 17 and 18, it

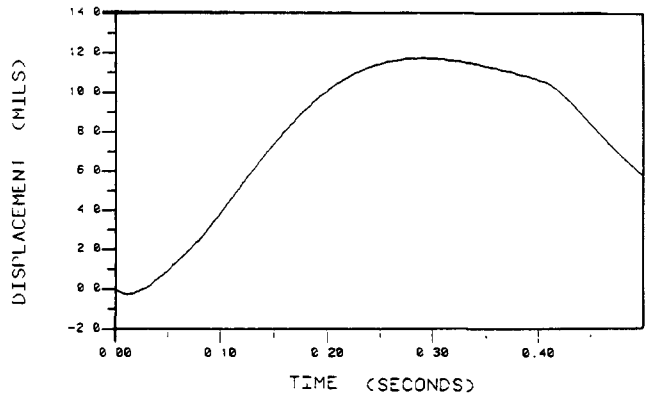

(*a*)

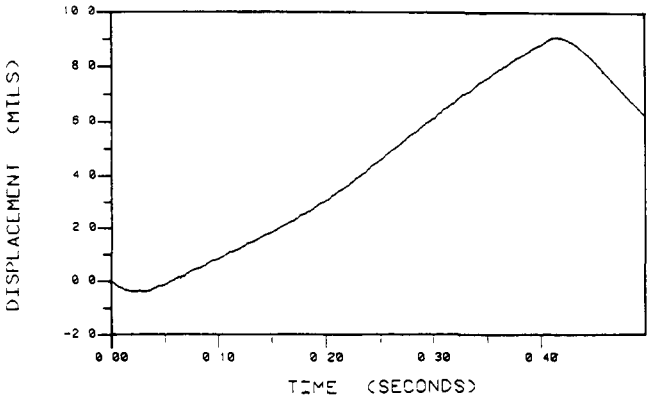

(*b*)

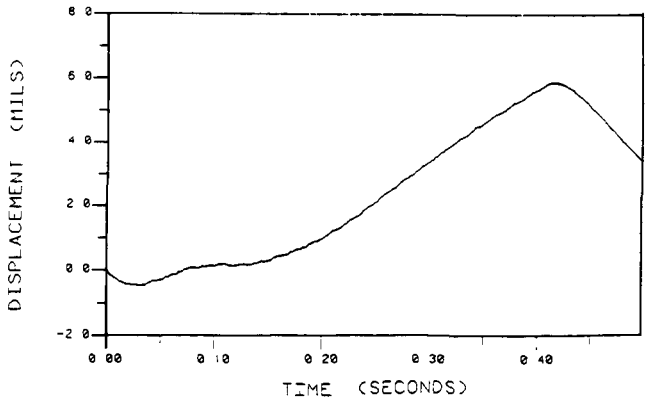

(*c*)

Fig. 18—(*a*) Dynamic displacement curve for uncoated steel (t. cone, 24 cycles, 9000 amps). (*b*) Dynamic displacement curve for galvannealed (t. cone, 24 cycles, 12,000 amps). (*c*) Dynamic displacement curve for hot-dip galvanized (t. cone, 24 cycles, 12,000 amps).

can be seen that the resistance curve of the uncoated material exhibits only regions 1, 6, 7, and 8 (as defined in Figure 30). The galvannealed coating exhibits all regions except 4 and 5, and the hot-dipped coating exhibits all 8 regions. The displacement curve of the uncoated material exhibits only regions 1, 4, 5, and 6. Both the galvannealed and hot-dipped coating exhibit all 6 regions, although regions 2 and 3 are not always pronounced for the galvannealed material.

Even though features in the displacement curves confirm the explanations being offered for the resistance curves,

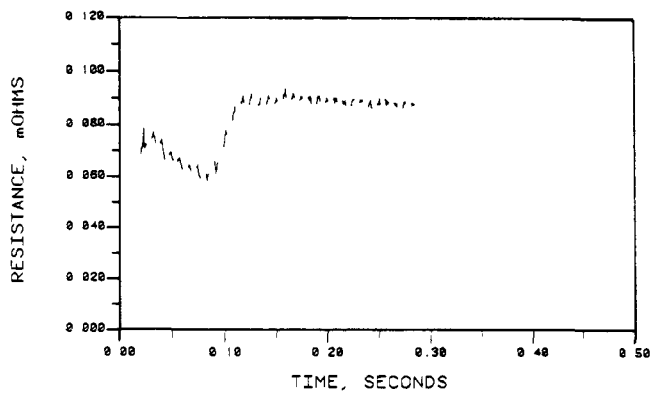

Fig. 19—Dynamic resistance curve for hot-dip galvanized with 4 cycles of upslope (t. cone, 12 cycles, 14,000 amps).

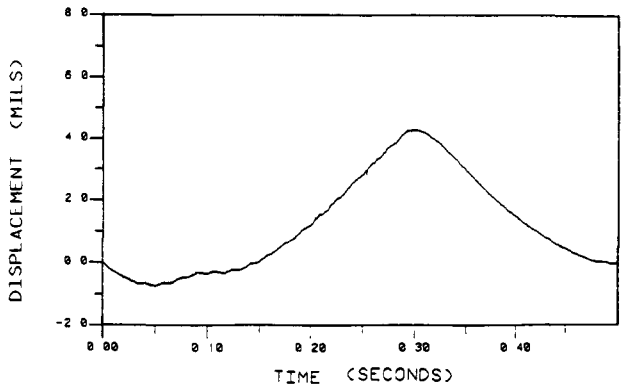

Fig. 20—Dynamic displacement curve for hot-dip galvanized with 4 cycles of upslope (t. cone, 12 cycles, 14,000 amps).

these curves will be discussed separately for clarity. There are a number of competing mechanisms responsible for the shapes of these curves. Resistive heating and thermal expansion can be counteracted by zinc movement and substrate softening. Even though the bulk resistivity is continually increasing with temperature, the contact resistance at each interface can be reduced greatly due to the presence of the molten zinc. The molten zinc halo can also increase the area of the current conducting channel. Occurrences at the faying and electrode interfaces need to be separately understood as well.

The mechanisms occurring during weld nugget formation will now be discussed as they affect the 8 regions of the generalized resistance curve (Figure 30).

Region (1) The initial steep fall in resistance is due to the breakdown of insulating films and asperity collapse. This must occur before any appreciable current can flow. This complex phenomenon involving surface film breakdown in a metallic contact is termed 'fritting'. As this portion of the curve is not actually measurable with the available experimental equipment, it has been drawn in Figure 30 with dashed lines.

Most metal surfaces, unless specially treated under ultra-clean conditions, are usually covered with insulating films of various contaminants, layers of oxide, and films of high resistivity. For most practical purposes, they are insulators and their presence at a contact interface enhances contact resistance. The theory of 'fritting' or electrical breakdown of such surface films suggests that a finite threshold voltage

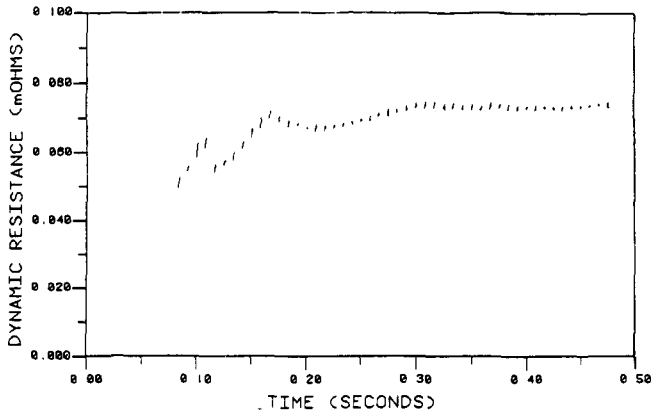

(a)

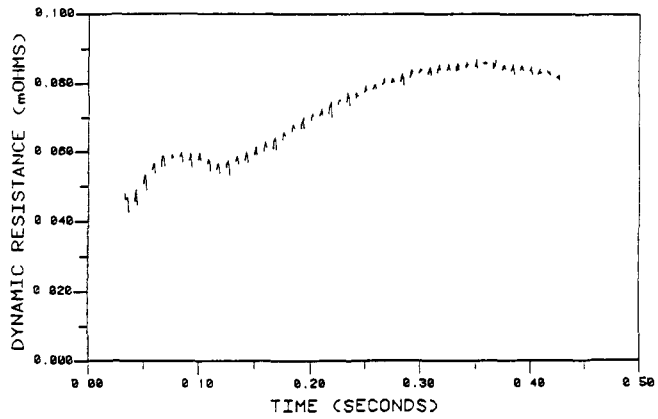

(b)

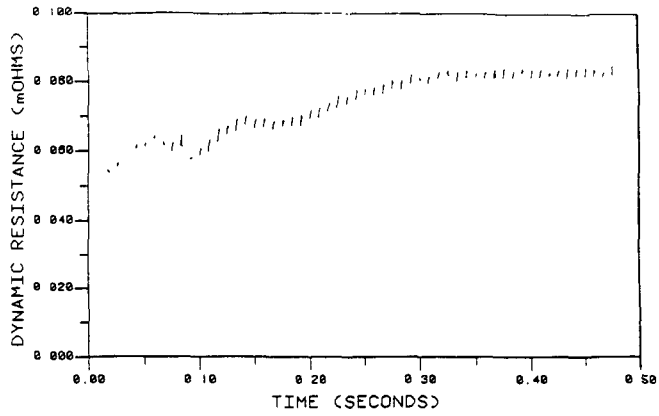

(c)

Fig. 21—(*a*) Dynamic resistance for hot-dip galvanized (radiused tip, 24 cycles, 14,000 amps). (*b*) Dynamic resistance for galvannealed (radiused tip, 24 cycles, 14,000 amps). (*c*) Dynamic resistance for hot-dip galvanized with 4 cycles of upslope (radiused tip, 24 cycles, 14,000 amps).

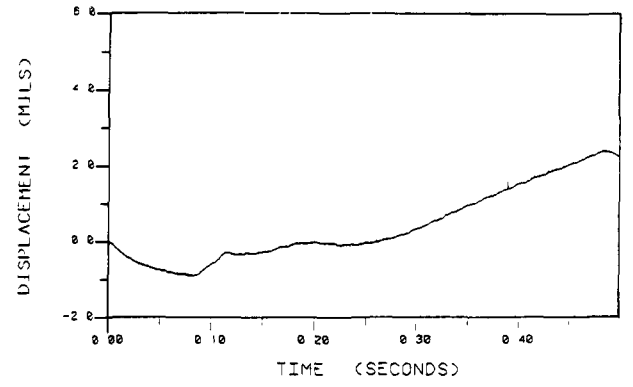

(a)

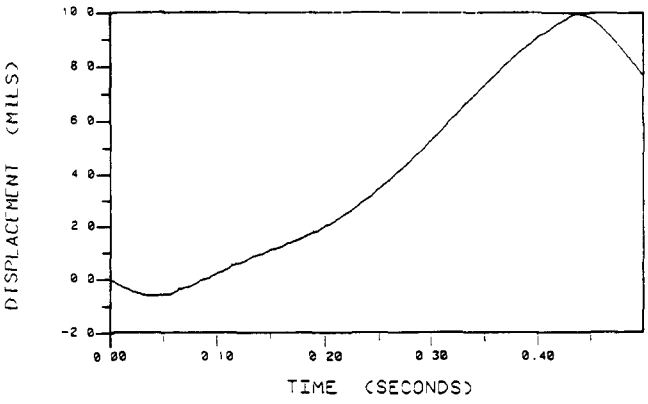

(b)

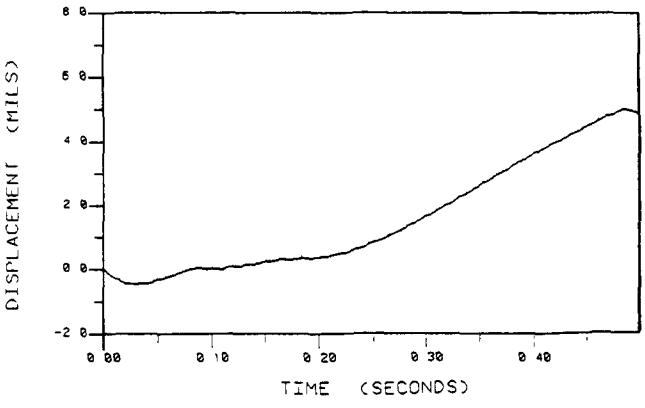

(c)

Fig. 22—(*a*) Dynamic displacement for hot-dip galvanized (radiused tip, 24 cycles, 14,000 amps). (*b*) Dynamic displacement for galvannealed (radiused tip, 24 cycles, 10,000 amps). (*c*) Dynamic displacement for hot-dip galvanized with 4 cycles of upslope (radiused tip, 24 cycles, 10,000 amps).

must be applied across the contact before any appreciable current can flow. This theory, proposed by Holm,[2] has been related to the resistance spot welding of uncoated materials by Bhattacharya and Andrews.[3]

Whenever two metals are brought into contact, their surfaces will touch only at points where the tips of asperities on one surface meet those of the other. With increasing pressure these asperities will flatten somewhat, but the actual points of contact will still be only a fraction of the apparent contact area. Once current begins to flow, the regions of point contact will heat up and soften, thereby allowing other asperities to touch and become heated. This process proceeds until the entire area of apparent contact becomes soft enough for all of the asperities to come into contact.

The phenomena of surface asperity breakdown constitutes the remaining portion of the fall in section 1 of the dynamic resistance curve. Note that fritting and breakdown of asperities occur at both the faying and electrode-sheet interfaces.

Table I. Effect of Zinc Location

Zinc Location	Lobe Width	Upsloped Width	Downsloped Width
Electrode interface	2000	2000	3000
Faying interface	1000	2000	2500
Both interfaces	1500	3000	2500
Uncoated	2500	2500	2500

This fall is much faster in the case of galvanized steel due to the softness and low melting temperature of zinc. Even though this phenomenon is of such short duration, it may have an influence on some of the longer time phenomena and lobe position.[4] It has been suggested[3] that fritting is largely responsible for increased peripheral heating which can be detrimental since the weld nugget should form in the center of the weld area rather than at the periphery. Figure 1 shows that melting is occurring at both the center and at the periphery, an indication that heating is not uniform at this early stage. The observation of peripheral melting has been observed previously in uncoated steels,[5] although the reasons given for its occurrence have varied.[2,6] Also, fritting and surface contaminants may form local hot-spots which may be detrimental to electrode tip life.

Region (2) The short rise in electrical resistance, which lasts for only the first cycle or two, is primarily due to bulk heating, not melting, of the zinc and Fe-Zn alloys on the electrode-sheet interface, although substrate bulk heating is also occurring. This is shown in the resistance curves in Figures 23(a) and 25(a) which compare the effects of zinc coating on either the faying or the electrode interfaces. As can be seen, the curve for zinc on the electrode-sheet interface has a large peak during this time. The results in Figure 27 also show this hump to be due to the coating at the electrode-sheet interface.

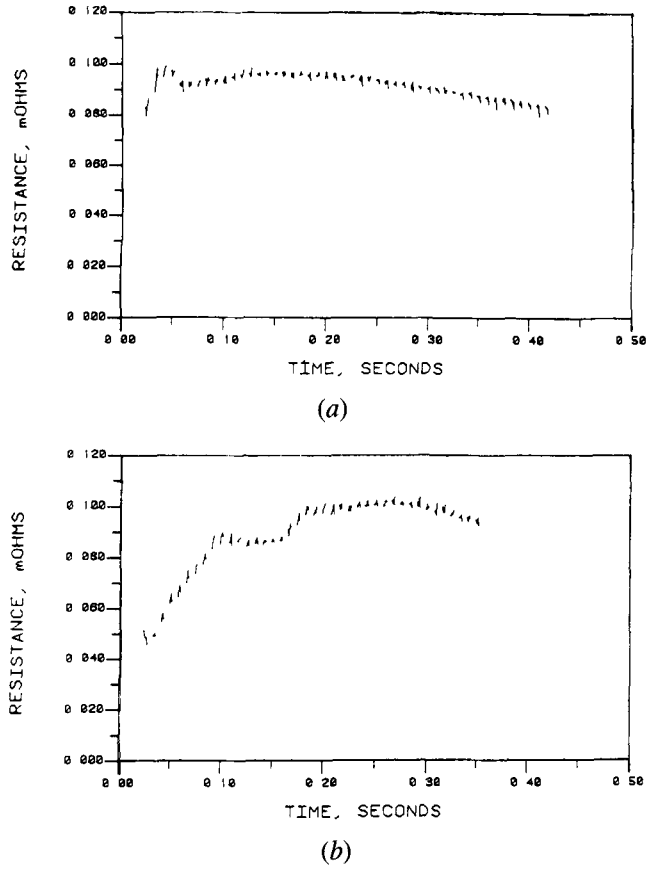

Fig. 23—(*a*) Dynamic resistance with zinc on electrode sides only (hot-dip, t. cone, 24 cycles). (*b*) Dynamic resistance with zinc on electrode sides only and 4 cycles upslope (hot-dip, t. cone, 16 cycles).

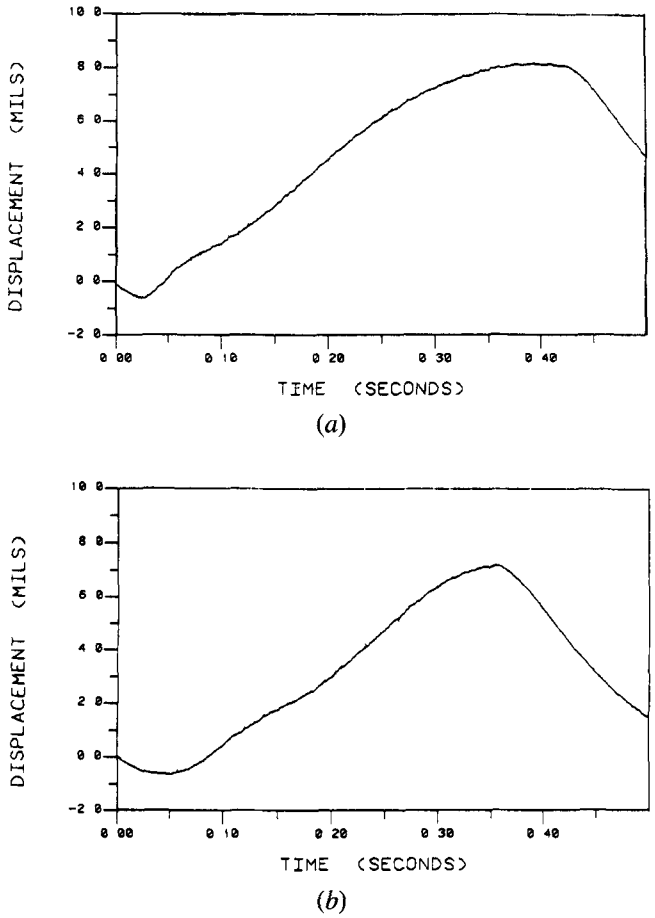

Fig. 24—(*a*) Dynamic displacement with zinc on electrode sides only (hot-dip, t. cone, 24 cycles). (*b*) Dynamic displacement with zinc on electrode sides only and 4 cycles upslope (hot-dip, t. cone, 16 cycles).

Figures 2 and 3 show that the zinc coating is being melted at the faying surface during the first cycle or two, whereas Figure 4 shows that little or no melting has occurred at the electrode interface after three cycles. A conductive liquid at the faying interface will greatly decrease the contact resistance. This explains why the resistance decreases initially in Figure 25(a) for zinc at the faying interface, and increases initially in Figure 23(a) for zinc at the electrode-sheet interface only. The total resistance is the addition of the series of resistances and therefore rises for a cycle or two for hot-dipped or galvannealed steel.

Region (3) The fall in dynamic resistance and ensuing valley, which form the remainder of the first hump (for coated materials), is due to the zinc becoming completely molten at both interfaces. The zinc which is now molten will decrease the contact resistance due to the intimate electrical contact that occurs with a liquid metal.

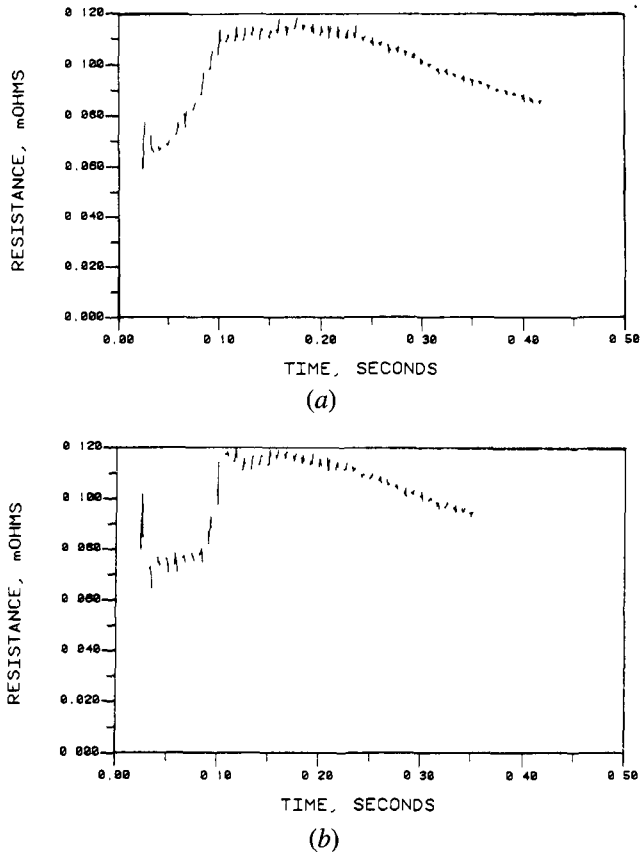

Fig 25 — (*a*) Dynamic resistance with zinc on faying sides only (hot-dip, t. cone, 24 cycles). (*b*) Dynamic resistance with zinc on faying sides only and 4 cycles upslope (hot-dip, t. cone, 16 cycles).

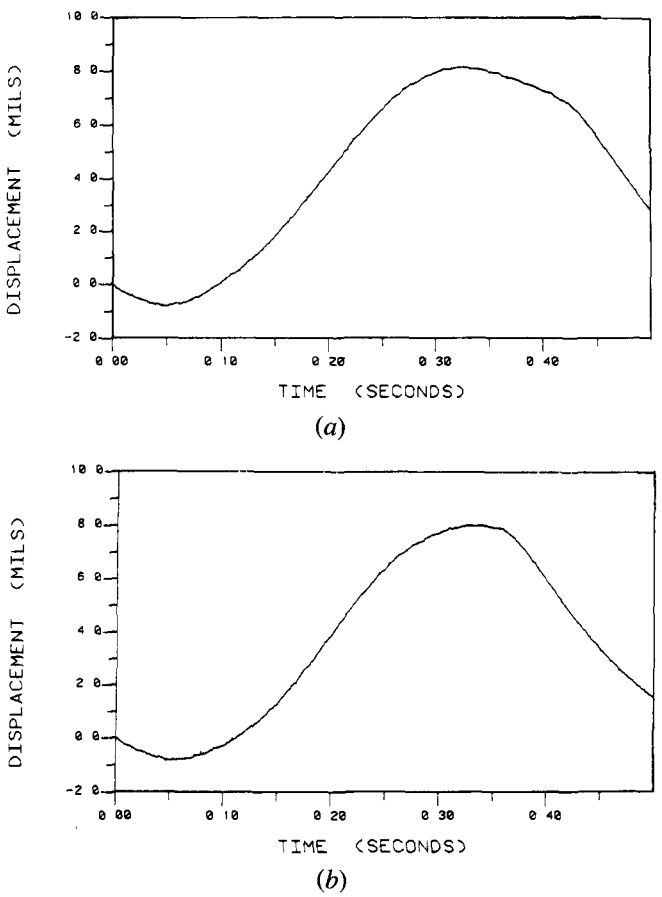

Fig. 26 — (*a*) Dynamic displacement with zinc on faying sides only (hot-dip, t. cone, 24 cycles). (*b*) Dynamic displacement with zinc on faying sides only and 4 cycles upslope (hot-dip, t. cone, 16 cycles).

The occurrence of molten zinc at both the faying and electrode interfaces has been well documented by Key and Upthegrove[7,8] and in our labs. High speed photography of a developing weld nugget, seen by cross-sectioning the electrodes and sheets to be welded, shows that the zinc becomes molten after only a few cycles. It has also been shown that for worn electrodes, the zinc at the electrode-sheet interface can become molten at an even earlier stage due to the increased resistance of the brass alloy which forms on the electrode.[9]

Work by Somsky[10] showed that the electrode-sheet interface does not become molten when welding uncoated materials. Zinc coating, on the other hand, does become molten at an early stage. This accounts for some of the differences in the dynamic resistance curves between uncoated and galvanized steels.

The decreased resistance caused by formation of molten zinc keeps the total resistance from increasing due to bulk heating of the steel substrate; however, this lasts for only a cycle or two. The molten zinc will then start to be forced from between the electrode tips to form a halo. The new iron contact and the continually increasing temperature causes the resistance to increase once again.

Region (4) The increasing bulk heating of the steel substrate soon overrides the decrease in contact resistance caused by the molten zinc. This results in an almost linear rise in the dynamic resistance. No melting of the steel substrate has begun at this time and there is still some free zinc remaining at both the faying and electrode-sheet interfaces.

Region (5) After about 6 cycles, most of the free zinc has been displaced and a mechanical seal starts to develop at the periphery of the electrode contact area. The seal is formed at both the faying and electrode-sheet interfaces. The electrodes are forced through the zinc coating at the periphery due to triaxial constraint of the zinc in the center. Also, Nied[6] has shown that there is increased pressure at the periphery at both the faying and electrode-sheet interfaces.

The seal which is formed traps the remaining zinc and weld metal between the electrode tips at both interfaces,

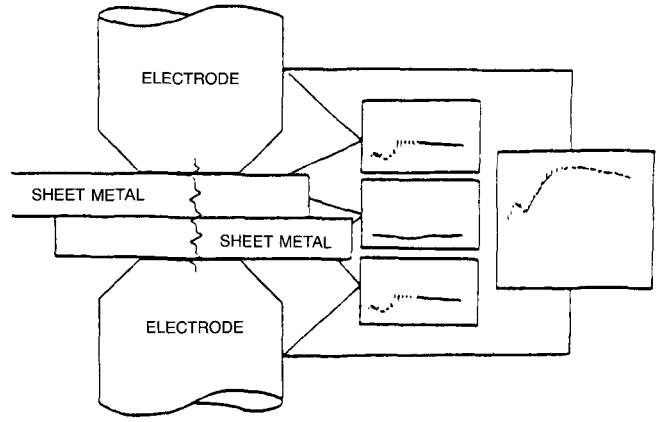

Fig. 27 — Dynamic resistance curves of the faying and electrode interfaces (hot-dip, t. cone, 24 cycles, 12,000 amps).

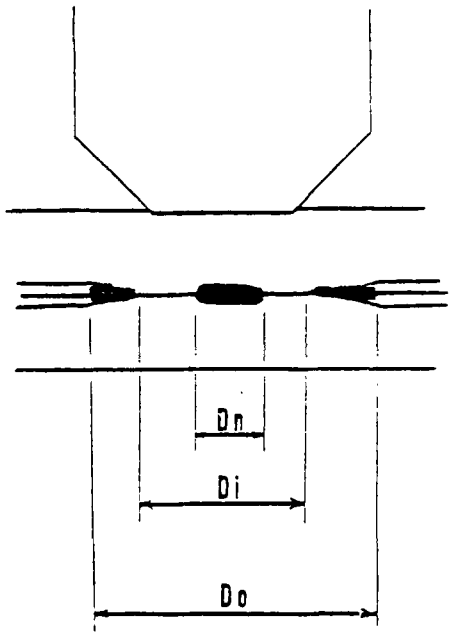

Fig. 28—Diagram of weld cross-section indicating the areas measured in the nugget and halo growth curves.

where the increased heat and pressure cause the zinc to combine with iron to form Fe-Zn alloys. This trapped zinc is seen in Figures 7(b) and 8.

The sudden increase in halo size with the formation of a seal at 5 or 6 cycles increases the area of current flow which decreases the total resistance between the electrode tips. The increase in halo size at this time is demonstrated by the halo growth curves in Figure 29. The zinc halo is an excellent conductor and helps lower the total resistance. Also, the movement of material from between the electrodes decreases the material thickness which decreases the resistance slightly.

This second hump is not seen for the galvannealed products because they do not exhibit this same phenomenon of halo growth. Uncoated material has no halo formation and hence no hump in the dynamic resistance curve.

It should be noted that the second hump can probably not be used as an accurate means of quality control. By inspection of Figure 32, one may be tempted to relate the movement of this hump to the size of the weld nugget; however, this hump may not always be present, especially under production conditions.[11] Furthermore, Figure 27 shows that much of the structure of the dynamic resistance curve is due to electrode-sheet phenomena rather than faying surface phenomena. Thus, monitoring dynamic resistance may give more information on electrode wear and bulk heating than a direct indication of nugget formation.

Region (6) This almost linearly rising section of the resistance curve is easily explained by the increased resistance due to heating of the iron-to-iron interface and bulk heating of the substrate. This feature has been explained by a num-

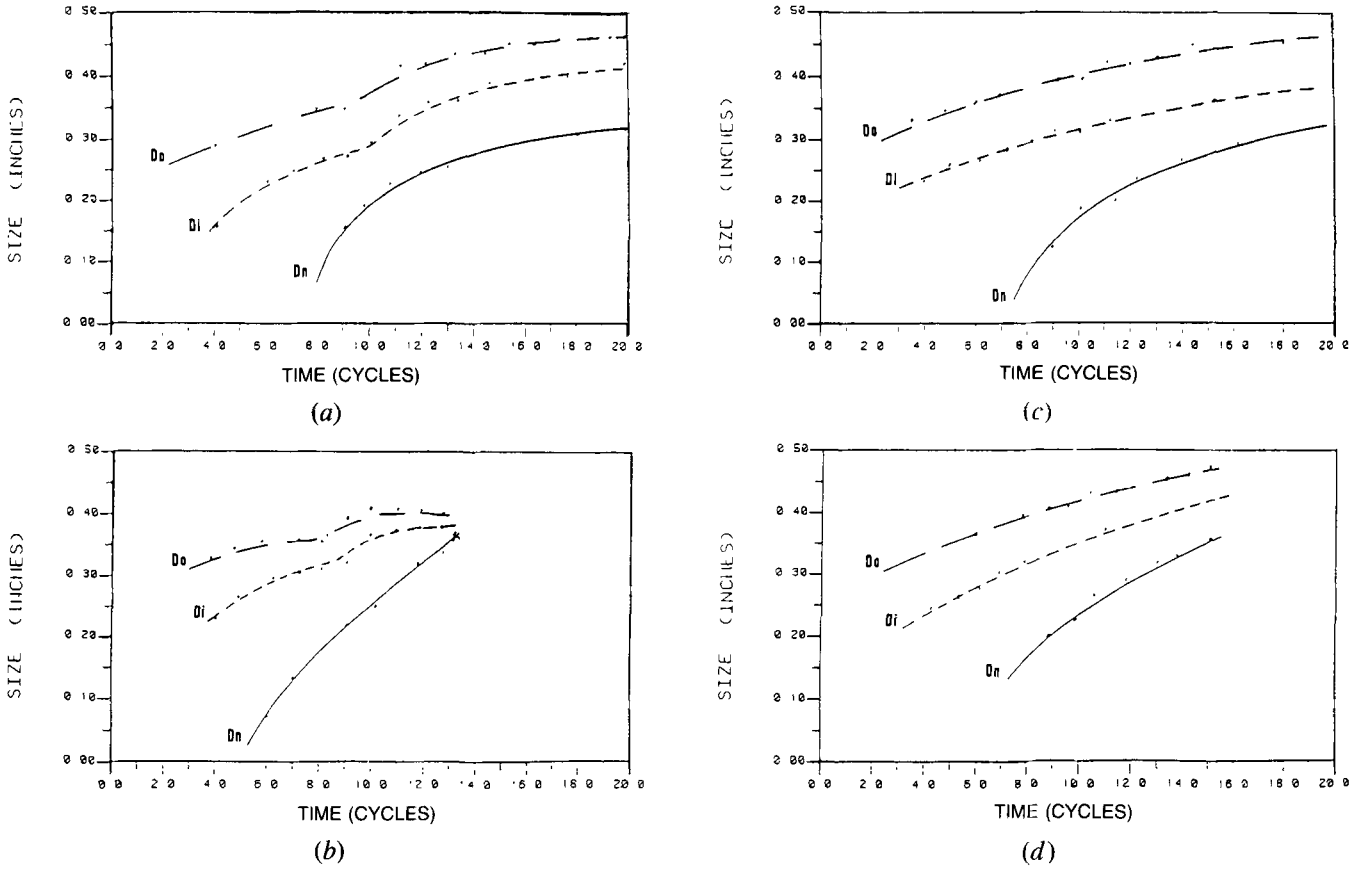

Fig. 29—(*a*) Nugget and halo growth curves for a weld which produces the minimum nugget size in 12 cycles (hot-dip, t. cone, 14,000 amps). (*b*) Nugget and halo growth curves for expulsion in 12 cycles (hot-dip, t. cone, 16,000 amps). (*c*) Nugget and halo growth curves for a 12 cycle minimum size weld with 4 cycles upslope (upsloped cycles included in time axis, hot-dip, t. cone, 13,000 amps). (*d*) Nugget and halo growth curves for expulsion in 12 cycles with 4 cycles upslope (upsloped cycles included in time axis, hot-dip, t. cone, 18,000 amps).

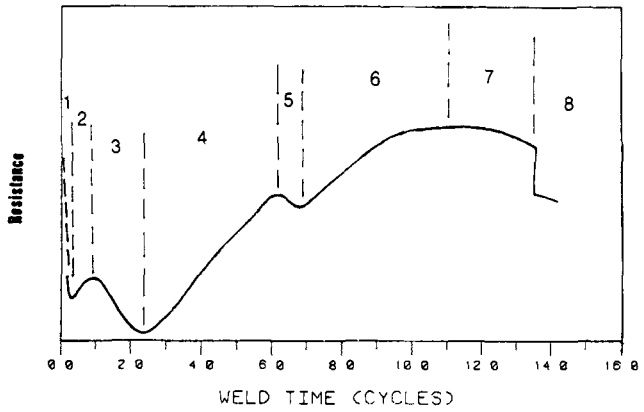

Fig. 30—Generalized resistance curve.

ber of investigators who have studied uncoated mild steel dynamic resistance curves.[5,12,13] The nugget begins to form near the end of this region.

Region (7) When a substantial amount of the metal reaches the melting or softening temperature, the slope of the dynamic resistance curve will decrease, and the resistance will reach a maximum and drop off. This is primarily due to collapse of the electrode-sheet interface and softening of the surrounding material such that the electrodes indent into the material. Also, this increases the halo area which increases the faying surface contact area and further decreases the resistance. Thus the total resistance will decrease due to the decrease in material thickness as well as an increase in the contact areas of the faying and electrode interfaces.

Bhattacharya and Andrews[3] have suggested that a melting voltage phenomenon takes place as well. This model is explained with the aid of Holm's theorem[2] but may not account for the full decrease in resistance as has been indicated by the work of Bowden and Williamson.[14] In any case, this does not significantly affect the interpretation of the dynamic resistance curve as it is presented by Bhattacharya and Andrews, which otherwise is in agreement with the present work.

Region (8) If material is abruptly expelled, the dynamic resistance will decrease sharply. This is due primarily to the abrupt loss of material thickness and extreme indentation. The sharp resistance drop is easily recognized and can be used in a quality control scheme to detect expulsion.

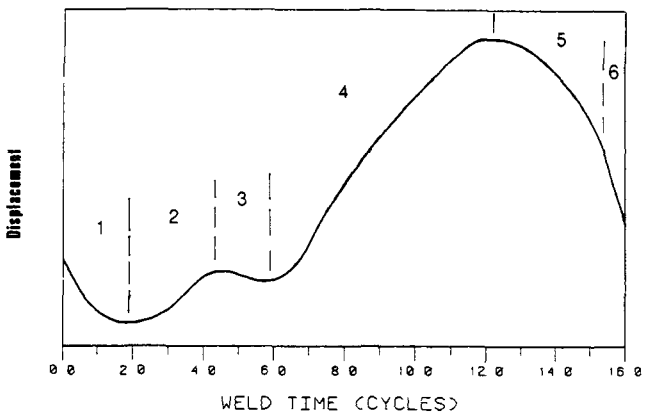

Fig. 31—Generalized displacement curve.

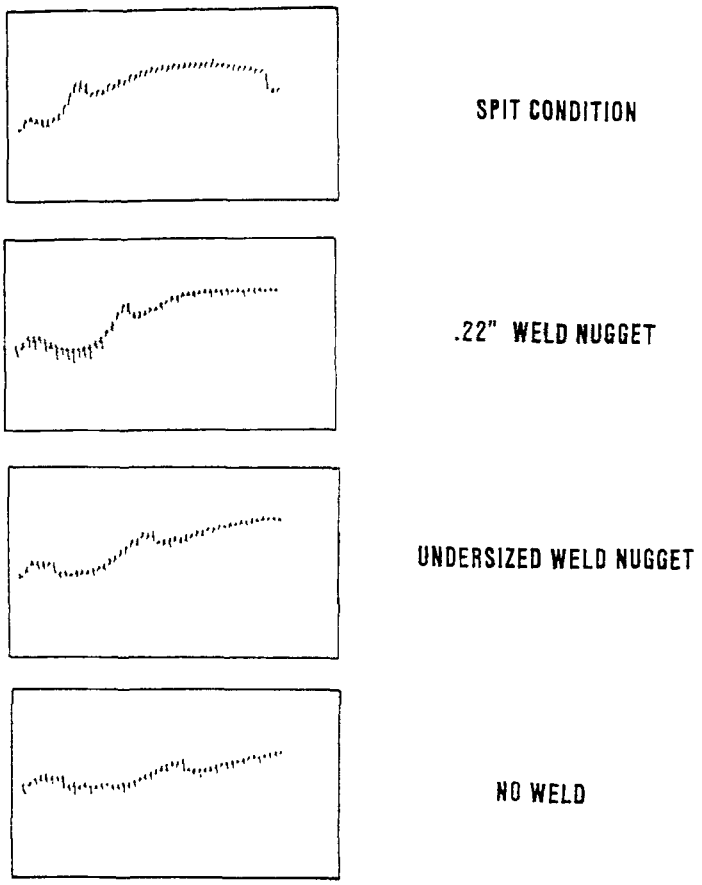

Fig. 32—Dynamic resistance changes with varying current (hot-dip, t. cone, 24 cycles).

In the discussion of region 5 it was mentioned that a seal began to form at the electrode periphery. This seal keeps the metal in place as it is heated to the softening temperature, melts, and forms a weld. The seal keeps the material from squeezing out radially as the molten zinc did earlier. As a result, the material is constrained and thermal expansion pushes the electrodes apart. Once this expansion becomes great enough, the seal is broken and the molten material is suddenly free to expel radially. The molten material is released with great force as the electrodes were compressing it at over 10,000 psi.

Another mechanism of expulsion occurs when the molten steel over 1500 °C gets close to the zinc which boils at 907 °C. This boiling zinc may force the electrodes apart and expel both zinc and iron.

The generalized displacement curve in Figure 31 has been separated into 6 distinct regions which will now be discussed separately. The discussion of the dynamic resistance curve will be incorporated into this discussion so that the two sources of information can be seen to complement each other. The dynamic displacement curves are easier to understand since there are basically only two competing mechanisms: thermal expansion, and removal of material (mostly zinc) from between the electrodes.

Region (1) The initial drop in the dynamic displacement curve is due to the flattening of asperities as the sheets are brought into contact. This initial drop may be larger if the material fitup is poor.

For the galvannealed and hot-dipped materials, the electrodes continue to move toward each other until a minimum is reached after one or two cycles of weld current. This continued drop is due to the easily softened zinc surface which can be pushed aside slightly in the first cycle or two before thermal expansion begins to dominate. The drop for galvannealed is much smaller than for hot-dipped since the Fe-Zn intermetallics are so much harder.

Uncoated material starts to expand almost immediately once the weld current starts. Thus the minimum in the displacement curve is reached at the end of the squeeze sequence. This occurs because there is no soft coating to push aside, and the thermal expansion of the steel substrate dominates the displacement trace immediately.

Region (2) Thermal expansion of the zinc coating as well as expansion of the substrate now begins to have a strong influence on the dynamic displacement trace. However, the zinc coating is also being slowly pushed from between the electrodes, especially from the faying interface, which permits the electrodes to close together instead of being pushed apart. As a result, the slope in region 2 is less than that of region 4 because of these two competing mechanisms. There is no region 2 in the dynamic displacement trace for the uncoated material.

This hump in the displacement curve is due almost entirely to heating and expansion of the zinc at the electrode interface rather than at the faying interface. The displacement trace of uncoated material is about the same as for material with zinc at the faying interface only, as is shown in Figures 24(a) and 26(a).

Region (3) The liquid zinc is now being pushed from between the electrodes faster than earlier in the weld. The zinc which was melting only moments before can now be pushed aside to form a halo. This occurs quickly enough to override the thermal expansion and result in a decrease in the total displacement. Figure 29 shows the increase in halo size at this time.

The displacement curves exhibited by galvannealed steels usually have a flat spot or simply a decreased slope rather than an actual hump in the displacement curve at this point. This is due to the thinner and harder coating on these steels which does not move aside as easily. The displacement curve of the uncoated materials show no humps or flat spots. This further supports the conclusion that the humps are due to movement of the zinc coating. Figures 24(a) and 26(a) show that this is due primarily to movement of zinc away from the electrode-sheet interfaces.

Region (4) As soon as the zinc coating is mostly removed from between the electrode tips and a seal has formed, the thermal expansion of the substrate material will again dominate the dynamic displacement curve. No more zinc can be pushed aside due to the formation of the seal. This nearly linear rate of expansion progresses until the material begins to soften or melt.

Region (5) Once the steel substrate begins to soften, the displacement slope will start to decrease. The electrode displacement will reach a maximum before the current is shut off if indentation of the electrodes begins to become prominent. Once the current is terminated, the displacement curve will begin to decrease as cooling occurs. In some longer time welds, or when using downsloping, the maximum will be reached before the current stops. In such cases electrode indentation may be substantial.

Region (6) If the weld current is too high or the time too long, expulsion will occur. The thermal expansion breaks the seal and material is expelled quickly as was discussed with respect to the resistance curve. Expulsion can easily be detected on a displacement trace by the rapid decrease as material is lost from between the electrodes.

In some cases, especially for very long times or excessive currents, expulsion can occur more than once. The electrodes will indent severely with the first expulsion, and the remaining material will then be subjected to continued heating. Since the material is already softened, expulsion can occur again easily.

Once the current is finally switched off, the material will cool quickly, and the displacement curve will drop smoothly. The final displacement will be less than at the start due to the permanent indentation of the electrodes.

B. *Effect of Process Modifications*

It was found that upsloping of the weld current increases the width of the current lobe when using truncated cone electrodes. This can be explained with reference to the mechanisms previously proposed. In addition, the evidence that upsloping can increase tip life can be explained.

The first hump in the dynamic resistance is more pronounced with upsloping. In particular, the valley is more pronounced (region 3 of the generalized resistance curve). By gradually increasing the current during upsloping, the zinc coating gradually heats up with little melting taking place. This develops a more favorable heat generation pattern by allowing the entire cross-section to rise in temperature before the zinc coating completely melts and decreases the faying surface contact resistance. It should be remembered that a high interface resistance is desired at the faying interface because that is where the weld nugget is expected to be formed.

When using upslope the second hump in the dynamic resistance is less obvious or even nonexistent, and the first hump in the displacement is less pronounced. This further supports the link between these two humps and can be explained by the fact that the zinc is being displaced more gradually when upsloping is used. The halo growth curves in Figure 29 show that there is no sudden increase in halo size in an upsloped weld because the heat is more evenly distributed throughout the material.

The seal which keeps the molten material in place between the electrode tips is formed more gradually and once formed is wider than that formed with no upsloping. The wider seal requires larger currents to produce expulsion.

Upsloping helps electrode tip life because the electrodes have a longer time to seat themselves into the zinc coating which decreases local overheating at asperity contacts. This, in turn, produces less heat at the electrode interface which makes zinc-copper alloying less pronounced. One might expect the beneficial effects of upsloping to be less on a welder of very low inertia where the electrode follow-up is very rapid.

If copper is being left on the zinc coated surface, then zinc is being deposited onto the copper electrode. Thus the amount of copper found in Figures 9 through 16 can give an indication of the magnitude of zinc-copper alloying to form brass on the electrodes. This, in turn, can give information on tip life and the mechanisms which affect tip life. Follow-

ing the suggestion provided by this study, several laboratories have studied the effect of upsloping on the electrode tip life and have confirmed that it is beneficial.[15,16]

C. *Effect of Using Radiused Tip Electrodes*

Radiused tip electrodes have been shown to increase the lobe width of materials with a free zinc coating when compared with truncated cone electrodes. It can be seen from the dynamic resistance curves in Figure 21 that the humps are more pronounced and that the second hump comes much earlier with radiused tipped electrodes. This occurs because the electrodes seat themselves more easily and push aside the zinc coating due to the curvature of the tips. This more efficient removal of zinc makes the second hump appear much earlier. Since the zinc coating is removed earlier, a weld nugget can form with less current. The expulsion current is also increased although the exact reason for this is not completely understood.

Upsloping does not increase the lobe width with radiused tip electrodes because the zinc is being pushed aside by the electrode geometry, and upsloping does not further enhance this. Also, a peripheral seal is not formed so that upsloping cannot make it thicker to repress expulsion. Radiused tips do not easily push aside the harder Fe-Zn alloys in the galvannealed material or the uncoated steel; therefore, they do not increase lobe width.

V. SUMMARY

An understanding of the mechanisms of nugget formation and growth can be gained through an analysis of dynamic inspection data in conjunction with a SEM study of developing weld nuggets. These mechanisms have been used to understand the effects of material variations or process modifications on galvanized steel.

It was found that features of the dynamic resistance and displacement curves can be explained by an understanding of the mechanisms responsible for their changing slope. The bulk resistance of the substrate continually increases with increasing temperature. This is opposed by decreases in resistance due to fritting, asperity breakdown, formation of intimate molten zinc contacts, and substrate softening and indentation. The displacement due to thermal expansion of the substrate constantly increases but asperity breakdown, movement of zinc away from the electrodes, and substrate softening and indentation cause a decrease in displacement. The different timing of these occurrences at the faying and electrode-sheet interfaces also affects the final shape of the dynamic resistance and displacement curves. In addition, process modifications such as upsloping can affect the shape of these dynamic monitoring curves.

ACKNOWLEDGMENTS

The authors wish to express their appreciation to Bethlehem Steel Corporation, General Motors Corporation, and the International Lead-Zinc Research Organization for their interest in and financial support of this work. Thanks also needs to be given to the undergraduate researchers who helped supply a large portion of the data in this study: C. Lane, J. LaPointe, K. Pate, S. Potter, D. Schrock, and K. Ulrich.

REFERENCES

1. J. J. O'Brien: "Adaptive Feedback Control for Galvanized Welding", Conf. Proc. Paper No. 20, Sheet Metal Welding Conf., AWS, 1984.
2. R. Holm: *Electric Contacts—Theory and Application*, Springer-Verlag, Berlin, Heidelberg, New York, 4th ed., 1967.
3. S. Bhattacharya and D. R. Andrews: "Significance of Dynamic-Resistance Curves in the Theory and Practise of Spot Welding", *Welding and Metal Fabrication*, Sept. 1974, vol. 42, pp. 296-301.
4. D. W. Dickinson and T. V. Natale: "The Effect of Sheet Surface on Spot Weldability", Transactions of ASM/ADDRG Conference, Dearborn, MI, April 14-15, 1981.
5. J. G. Kaiser, J. G. Dunn, and T. W Eagar: "The Effect of Electrical Resistance on Nugget Formation during Spot Welding", *Welding Journal*, June 1982, vol. 61, pp. 167s-74s.
6. H. A. Nied: "The Finite Element Modeling of the Resistance Spot Welding Process", paper presented at the 64th AWS annual meeting held in Philadelphia, PA, April 1983.
7. J. F. Key: "A High Speed Photographic Analysis of Spot Welding Galvanized Steel", Master's Thesis, University of Texas at Austin, Aug. 1970.
8. W. R. Upthegrove and J. F. Key: "A High Speed Photographic Analysis of Spot Welding Galvanized Steel", *Welding Journal*, May 1972, vol. 51, pp. 233s-44s.
9. S. L. Roswell: "Resistance Welding of Hot-dipped Galvanized Steel", *Metal Construction*, April 1978, vol. 25, pp. 163-69.
10. P. Somsky: "Special Features of the Formation of the Weld Nugget in the Resistance Spot Welding of Galvanized Sheets", *Zvarnie*, 1972, vol. 21(6), pp. 172-75.
11. D. Watney and G. L. Nagel: "Forms of Dynamic Resistance Curves Generated during Resistance Spot Welding", Proc. Conf., Paper No. 14, Sheet Metal Welding Conference, AWS, Dearborn, MI, Oct. 1984.
12. D. W. Dickinson: "Welding in the Automotive Industry", Committee of Sheet Steel Producers, Research Report SG81-5, August 1981.
13. D. W. Dickinson, J. E. Franklin, and A. Stanya: "Characterization of Spot Welding Behavior by Dynamic Electrical Parameter Monitoring, *Welding Journal*, June 1980, vol. 59, pp. 170s-76s.
14. F. P. Bowden and J. B. P. Williamson: "Electrical Conduction in Solids-I. Influence of Passage of Current on the Contact between Solids", Proceedings of the Royal Society, 1958, vol. 246A, pp. 1-12.
15. D. Watney: development engineer, General Motors Corporation, Warren, MI, 48090-9040, unpublished research, 1984.
16. J. Sawhill, Jr.: senior engineer, Bethlehem Steel Corporation, Bethlehem, PA, 18016, unpublished research, 1984.